GATING CURRENT HARMONICS

I. Sodium Channel Activation Gating in Dynamic Steady States

JURGEN F. FOHLMEISTER*‡ AND WILLIAM J. ADELMAN, JR*

**Laboratory of Biophysics, National Institute of Neurological and Communicative Disorders and Stroke, National Institutes of Health at the Marine Biological Laboratory, Woods Hole, Massachusetts 02543; and ‡Laboratory of Neurophysiology, University of Minnesota, Minneapolis, Minnesota 55455*

ABSTRACT Internally perfused and pronase-treated giant axons were prepared for gating current measurements. Gating current records were obtained under large-amplitude sinusoidal voltage clamp after allowing for settling times into dynamic steady states. The current records were analyzed as functions of the mean membrane potential of the test sinusoid for which the amplitude and frequency were held constant. The nonlinear analysis consisted of determining the harmonic content (amplitudes and phases) of the distorted periodic current records. The most pronounced feature found in the analysis is a dominant second harmonic centered at $E_{mean} = +10$ mV. A number of other characteristic harmonic behaviors were also observed. The harmonics tend to die away for very small (< -60 mV) and very large ($> +72$ mV) values of E_{mean}. The harmonic behavior seen in the axonal data is basically different from that seen in gating current simulations generated by the sodium-activation kinetics of standard models, including the Hodgkin-Huxley model. Some of the differences can be reconciled without requiring fundamental changes in the model kinetic schemes. However, the dominant harmonic feature seen in the axonal data cannot be reconciled with the model kinetics without a fundamental change in the models. The axonal data suggest two moving molecular components with independent degrees of freedom whose properties are outlined on the basis of the data presented herein.

INTRODUCTION

Gating current, also called asymmetry current, is a component of the dielectric displacement current of excitable membranes that is correlated with activation gating of the voltage-sensitive sodium channels (Keynes and Rojas, 1976; Bezanilla and Armstrong, 1977; Taylor and Bezanilla, 1983). In this paper and in the companion paper Fohlmeister and Adelman (1985), gating currents are assumed to be the reasonably direct external expression of certain conformational changes within the channel molecule or of realignment among channel subunits. This current thus provides a window on the activation gating process that is used to obtain information about the nature of the transitional kinetics.

To exploit this window the currents must be elicited by judiciously chosen patterns of changes in the transmembrane electric field. Although the molecular equilibrium states are not likely to form a continuum, the number of local energy minima can nevertheless be quite large. Thus, gating current is likely to be the external expression of a temporal sum of elementary transitions among the energy minima. The key to resolving these transitions lies in finding a set of voltage stimuli, each member of which causes a different temporal pattern among the transitions. The approach taken in this set of papers is to generate these patterns of transitions in different but largely overlapping voltage domains; the conformational states that are dominantly populated will change from one domain to the next. Therefore, the relative importance of each possible transition in contributing to the gating current will also change from one domain to the next.

The voltage stimuli we use are relatively large amplitude (70 mV peak to peak) sinusoids about a set of mean membrane potentials, E_{mean}. The value of E_{mean} defines each voltage domain. Following the onset of the sinusoid the system will approach dynamic steady state. In that state the molecules will respond with periodic conformational movement. The specific form of the periodic movement is determined by the kinetic scheme of the voltage-sensitive process; the associated gating current will be distorted according to the particular internal kinetic feedback patterns thus established.

The distortion is measured relative to the sinusoidal waveform of the command voltage. We use harmonic analysis because any nonzero harmonic component is a

Send correspondence to Dr. Jurgen Fohlmeister, Physiology Department, 6-255 Millard Hall, 435 Delaware Street, SE, University of Minnesota, Minneapolis, MN 55455

measure of the distortion. We find that a number of diverse models of gating (e.g. two versions of conformational kinetics based on the Hodgkin-Huxley model, models of aggregation gating, models containing kinetic loops or branches) all yield a basically similar pattern of the harmonic content as a function of E_{mean}; a pattern that is fundamentally in disagreement with the data. That disagreement is resolved by Fohlmeister and Adelman (1985), by introducing kinetics that are dynamically equivalent to the data and that reproduce those experimental phenomena for which the classical models were designed.

METHODS

Preparation and Voltage-Clamp Commands

Cleaned single giant axons from the hindmost stellar nerve of the squid *Loligo pealei* were internally perfused and voltage clamped. The waveform of the voltage-clamp command pulses consisted of a step from the holding potential of −70 mV to one of a set of mean membrane potentials that was held constant for 1 ms. Immediately following this constant level the voltage was varied sinusoidally with an amplitude of ±35 mV (70 mV peak to peak) about the same mean membrane potential (Fig. 1) and with a frequency in the range of 500 Hz to 5 kHz. The duration of the sinusoidal waveform was 16 ms, after which the voltage was stepped back to the holding potential. The set of mean membrane potentials consisted of values spaced by 4 to 8 mV in the range from −112 to +76 mV, plus the value of −160 mV, which served as subtraction holding potential. The pulses, which were spaced by 2 s, were generated in groups of eight consisting of four pulse pairs. Each pair consisted of a test pulse and a subtraction (control) pulse. Within each group of eight the mean level of the four test pulses was held constant. Furthermore, the frequency and amplitude of the sinusoid were held constant for all eight pulses within the group. The current records generated by the control pulses were subtracted from those generated by the test pulses and the resulting four current differences were then averaged. Further signal averaging was subsequently achieved by folding the averaged current difference onto a single period equal to that of the command sinusoid (see Analysis of Current Records below). Temperature was 7.9 ± 0.1°C.

Solutions

Each axon was prepared for voltage clamp by a series of solution changes. The initial perfusion was carried out with the axon bathed in artificial sea water (ASW) and the perfusate was Na^+-free and contained 300 mM K^+ and 505 mM sucrose (see Table I). At this point each axon was checked for its ability to generate an action potential of at least 100 mV in response to a depolarizing current shock to <10 mV above the resting potential. With the clamp circuit remaining open, the above mentioned internal solution was then supplemented with protease (type XXI; Sigma Chemical Co., St. Louis, MO) to a concentration of 1 mg/ml. During the following 10 min, the electrical properties of the axon were observed to undergo a series of changes: The first noticeable change was that action potentials generated in response to a depolarizing current shock began to develop increasingly long plateaus during their falling phases (c.f. Fig. 2 *A*). After ~4 min the axons became spontaneous, generating trains of plateau action potentials at a frequency of ~40 impulses/s without external electrical stimulus. This spontaneity was rhythmic in that the membrane potential would periodically remain at the plateau level (about −22 mV) of the action potentials for ~30 s before becoming oscillatory again. Each consecutive train (which also had a duration of ~30 s) of plateau action potentials followed the same qualitative development: it began with a slow decline from the plateau level towards more negative membrane potentials followed by a broad and small amplitude action potential. The amplitude of the subsequent plateau action potentials then increased until the membrane potential again held at the plateau value of the last impulse in the train.

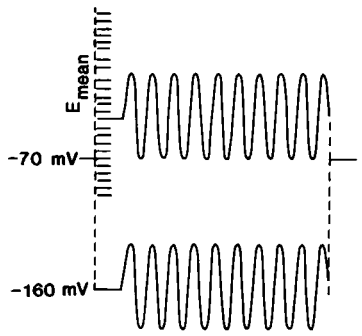

FIGURE 1 Command voltage profiles. The asymmetry (gating) currents are defined as the difference of the current responses between the *upper* and the *lower* command signal of equal frequency, amplitude and phase. The two commands were spaced by 2 s.

After 10 min of protease treatment the internal solution was changed to a K^+-free, protease-free solution containing Cs^+ as its principal cation (see Table I) and the axon was voltage clamped with a depolarizing square-wave pulse. The purpose of this pulse was to check the degree of the absence of Na inactivation as judged by the falling phase of the current record (Armstrong, Bezanilla, and Rojas, 1973). In general we found that ~75 to 80% of the inactivation had been removed at this stage. Satisfied with the state of health of the membrane and with the degree of progress, we switched back to the original protease-containing internal solution for an additional 4 to 5 min. At this point we switched (normally for the last time) to the experimental K^+-free and protease-free internal solution and found that the Na inactivation had been virtually fully removed (the current records showed no falling phase following step depolarizations). The membrane was held in clamp at −70 mV from this point forward and the external solution was changed to the Tris-TTX-seawater solution listed in Table I. This external solution was daily prepared anew. The final, experimental solutions were K^+-free, contained 10 mM Na^+ each and contained $Tris^+$ as their principal external cation and Cs^+ as their principal internal cation. A measured electrode junction potential of +3 mV was compensated.

TABLE I
COMPOSITION OF SOLUTIONS

	External Solutions (in millimoles per liter)						
	Na	Ca	Mg	Tris‡	Cl	TTX	
ASW*	430	10	50	10	570	—	
Tris-TTX-SW	10	10	20	435	505	0.0005	
	Internal Solutions (in millimoles per liter)						
	Na^+	Cs^+	K^+	F^-	HPO_4^{-2}	Glut.$^-$	Sucrose‖
300 K§	—	—	300	50	25	200	505
190 Cs 10Na	10	190	—	180	10	—	590

*plus 10 mM K^+.
‡Tris (hydroxymethyl) aminomethane.
§Pronase (Sigma Chemical Co., type XXI) was added to this solution during preparation to the extent of 1 mg (pronase)/ml.
‖This concentration of sucrose gave an osmolarity of 980 mOsmol/kg.

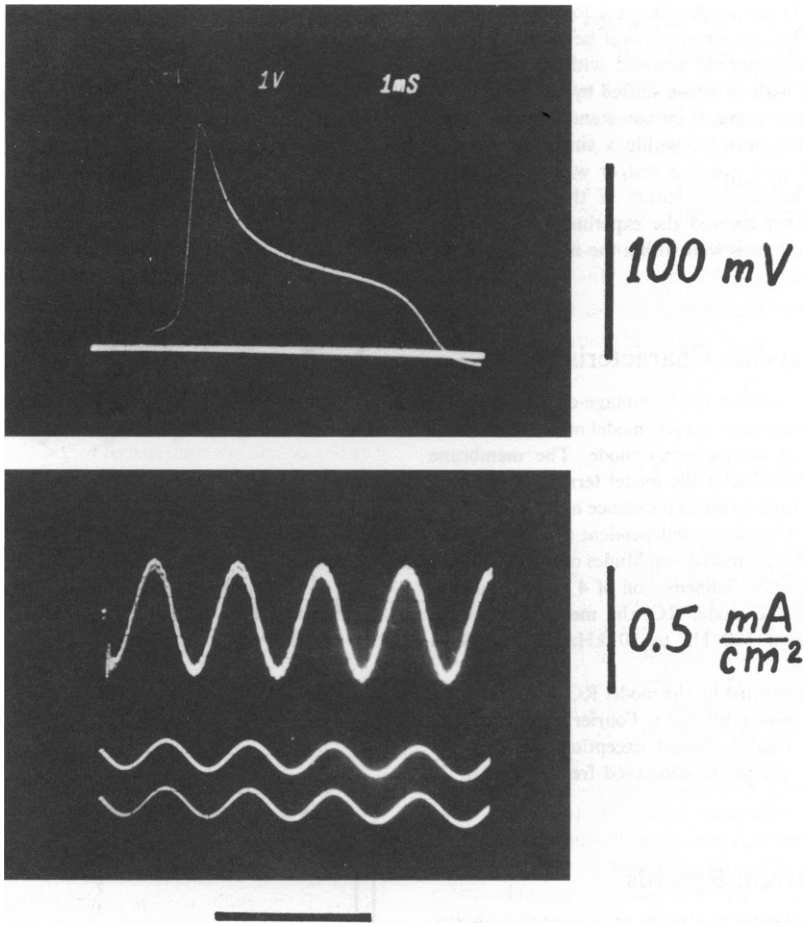

FIGURE 2 (*A*) Plateau action potential generated by an axon internally treated with pronase for 4 min. The rising phase was drawn in by hand because it was too rapid to be recorded on the storage oscilloscope.
(*B*) Current (*upper* pair), and command voltage traces (*lower* pair) at a frequency of 0.95 kHz. Solutions were the Tris-TTX-SW and the 190 Cs 10 Na listed in Table I. Horizontal bar is 4 ms for *A*, and 2 ms for *B*.

Series Resistance Compensation and Space Clamp

A measured series resistance of 2.4 Ω cm² was fully compensated. For details of the method of series resistance compensation, as well as details of the experimental chamber and electrodes as they relate to longitudinal electrical averaging (space clamp) see Methods in Fohlmeister and Adelman (1984).

Synchronization and Stability

Following the current-to-voltage conversion of the membrane current, the data were digitized at 5 μs intervals. Since the gating current data are the difference between two current records obtained with sinusoidal voltage-clamp commands (c.f. Fig. 2 *B*), it was of primary importance to synchronize the sampling times of the analog-to-digital (A/D) converter with a fixed phase of the command sinusoid. Otherwise (as, for example, with a free-running A/D converter) the test and control currents would be sampled at slightly different phases, the phase difference varying randomly from one experimental pulse to the next. Since the (capacitative) currents generated in each pulse are essentially sinusoidal in time, taking the difference of two such records introduces an artifactual, sinusoidally varying component with a frequency equal to that of the command sinusoid, but phase shifted by ±90 degrees relative to the individual sinusoidal current records. The amplitude of this artifact depends directly on the phase difference in the sampling points of the test and control pulses. To see this, consider the difference of two sine waves with equal amplitude and frequency but sampled at points shifted in phase by the small amount ϵ:

$$
\begin{aligned}
&A \sin \omega t - A \sin (\omega t \pm \epsilon) \\
&\quad = A [\sin \omega t - \sin \omega t \cos \epsilon \mp \cos \omega t \sin \epsilon] \\
&\quad = A [\sin \omega t - [1 + 0(\epsilon^2)] \sin \omega t \mp [\epsilon + 0(\epsilon^3)] \cos \omega t] \\
&\quad = \mp \epsilon A \cos \omega t.
\end{aligned}
$$

This small amplitude cosine component is strictly a sampling artifact; it cannot be detected in, or removed from, a data record. To allow it would be intolerable because its amplitude is of the same order as the amplitude of the gating current. For this reason, great care was taken to electronically trigger the command sinusoid and the sampler of the A/D converter with the same clock. The effectiveness of this synchronization was checked by (sinusoidally) voltage clamping a model RC circuit and taking the difference of two digitized current records. The difference was flat to well within the noise level (see below). In tests with a free-running sampler of the A/D converter the artifactual cosine component was nearly always present.

These tests on a model membrane RC circuit confirmed two further important requirements of the voltage-clamp system; these are its ampli-

tude and frequency stability. If the amplitude were to change slightly from one pulse to the next, that occurrence would be detected in the current difference as a small amplitude sinusoid with the command frequency, and either in phase with, or phase shifted by 180° relative to the phase of an individual current record. If the command frequency were changing from one pulse to the next (or within a single pulse), that occurrence would be detected as a growing and/or waning sinusoidal current difference (or beat frequency). Neither of these effects was observed in numerous trials that covered the experimental frequency range, and their presence, if any, was well within the noise level of the current-difference records.

Frequency Response Characteristics

The frequency response characteristics of the voltage-clamp system to sinusoidal commands were measured on the RC model membrane circuit in the passive (low membrane conductance) mode. The membrane potential and current were monitored at the model terminals. With no series resistance compensation (and no series resistance in the model RC) the voltage amplitude remained frequency independent and 100% in the range from 100 Hz to 10 kHz for command amplitudes of ±20, ±50, and ±200 mV. With a series resistance compensation of 4 Ω cm^2 and that series resistance switched into the model RC, the membrane voltage amplitude remained 100% from 100 Hz to 10 kHz for command amplitudes of ±20 and ±50 mV.

Individual current records generated by the model RC for frequencies within the experimental range were subjected to Fourier analyses. These tests produced the following results without exception: the analyses showed a fundamental component at the command frequency with all harmonics at the noise level.

Analysis of Current Records

Following the computer acquisition of the digitized current records the data were reduced in the following series of steps by the PDP 11-60 (Digital Equipment Corp., Maynard, MA) laboratory computer:

(*a*) The control record was subtracted from the test record point by point for each record pair (see Preparation and Voltage-Clamp Commands, above).

(*b*) The data from four record pairs were averaged point by point (ibid.). Examples of the results of this step are given in Figs. 3, 4, and 5 in the Results.

(*c*) For reasons given below, nine additional points were inserted between every two consecutive data points (after averaging) and equally spaced by linear interpolation.

(*d*) The data array from step *c* (now 10 times as long as the array from step *b*) was divided into segments, each corresponding in length to precisely one period of the command sinusoid. That period was measured during data acquisition by an electronic counter (DC 504; Tektronix Inc., Beaverton, OR) connected to the command function generator (FG 501; Tektronix Inc.). The counter gave a single value to the nearest microsecond of the average sine-wave period during each voltage-clamp pulse. We therefore acquired eight measures of that period for each group of eight pulses that were subtracted and averaged in steps *a* and *b* above. The microsecond digit of the counter normally changed between two consecutive integers from one pulse to the next in a random fashion. With eight measurements, we therefore felt confident in estimating the period to the nearest 0.5 μs. The resulting value of the period was entered in the computer for purposes of dividing the data array.

(*e*) The first 4 ms were discarded to allow settling time into dynamic steady state. This time was established as follows: Individual segmental records for all values of E_{mean} and command frequency were subjected to harmonic analysis. Segments that occurred at least in part within the first 2 ms of the total record showed systematic changes in harmonic content. Segments that occurred outside of that range showed only small and random changes in their harmonic contents. Thus, 4 ms was established as the time after which all segments were fully beyond the initial 2 ms for the lowest experimental command frequency. For most of the experimental frequencies this criterion provides an additional margin of settling time into a state that is approached asymptotically.

(*f*) The remaining complete segments were overlayed and averaged, resulting in a further enhancement of the signal-to-noise ratio.

(*g*) The single period of data resulting from step *f* was then subjected to

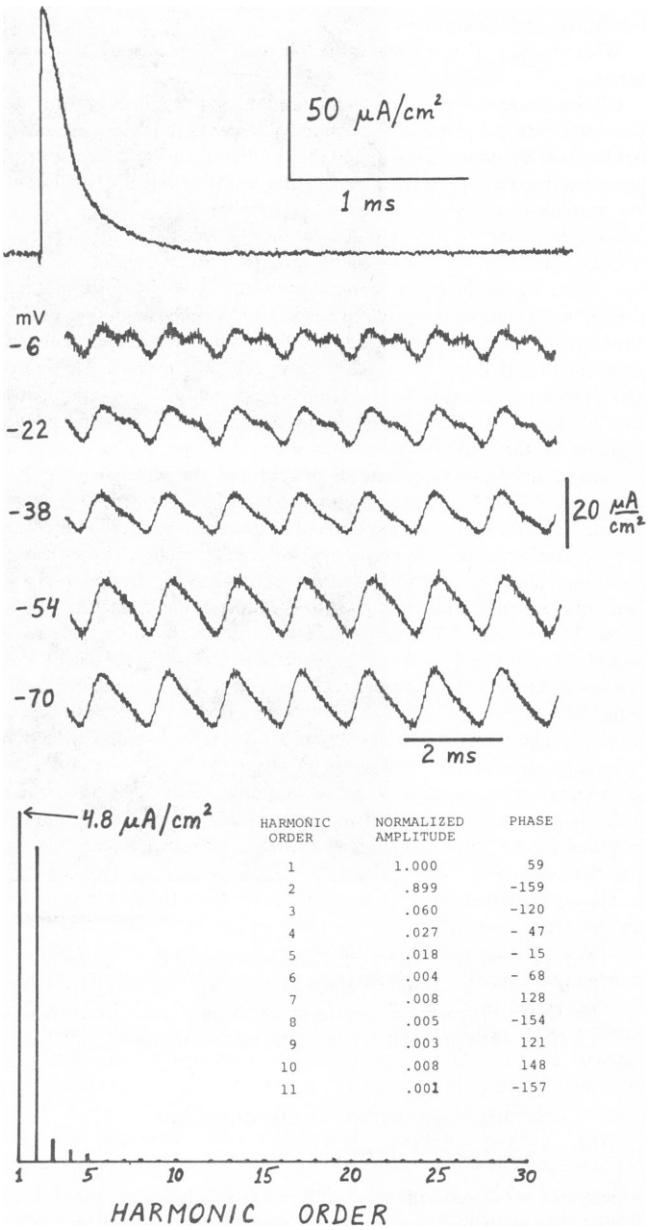

FIGURE 3 *Upper* trace: Gating current transient in response to a voltage step from −70 to 0 mV (see text for further details).
Central traces: Periodic gating current records in response to sinusoidal voltage clamp at 730 Hz and ±35 mV amplitude for five values of E_{mean} given at the *left*. The records are signal averages of 21 voltage-clamp pulse pairs (see text).
Bottom panel: Amplitudes of the fundamental and harmonic components of the record for $E_{mean} = -6$ mV given in the *central* panel. Table gives the corresponding normalized amplitudes and phases.

a fast Fourier transform (FFT) routine to extract the fundamental component and the harmonic content.

With regard to this procedure the following two points are of importance:

(*i*) Great care was taken to synchronize the sampling times of the A/D converter with the phase of the command sinusoid to avoid a sampling artifact (see Synchronization and Stability, above). However, because the sampling frequency (200 kHz) was not, in general, an integral multiple of the command sine-wave frequency, a sampling artifact may still be introduced during the folding process of the digitized current data (step *f* above). The effect of this sampling artifact is to decrease the higher harmonics by producing a random back and forth jitter during the overlaying of individual record segments. To reduce the amplitude of this jitter by a factor of 10, nine additional points were inserted between consecutive data points in the data array, step *c* above. The insertion of those points reduced the effective sampling interval to 0.5 μs, and allowed the full use of the accuracy of the measured sine wave period in the dividing of the current record into segments (step *d* above). For a command sine-wave frequency of 5 kHz and the effective sampling frequency of 2 MHz, the maximum phase error from segment to segment is reduced to 0.9°. For lower command frequencies the maximum phase error is further reduced in proportion with the frequency. However, the maximum phase error of the harmonics is equal to the maximum phase error of the fundamental multiplied by the order of the harmonic.

(ii) To take the FFT (step *g*) the folded, single period data record is sampled at a number, N, of equally spaced points covering the period. For a given N, harmonics up to order $N/2$-2 are computed. We chose $N = 64$, which yielded harmonics up to the 30th order. To determine the 64 values from the folded data record the computer was programmed to divide the externally supplied sine-wave period by 64 and to pick off values from the data record at the resulting intervals. However, because the 64 markers will, in general, each fall between two record points, the 64 values required for FFT were determined by linear interpolation between the two flanking record points.

Having arrived at the array of 64 values, one faces the problem of noise in the data record. However, low-order harmonic analysis is virtually unaffected if one, several or all of the $N = 64$ values of the array are randomly displaced in amplitude; only systematic displacements throughout the period enter the low-order harmonics. Random displacements enter as contributions to higher harmonics, which are discounted in the present analysis. This property of harmonic analysis is commonly exploited for image enhancement of noisy photographic and other image data.

As a test of this property we reduced the noise level by signal-averaging 21 pulse pairs (instead of four pulse pairs) at a relatively low command frequency (730 Hz) prior to the folding step. The resulting records for five values of E_{mean} are given in Fig. 3. Note the substantially reduced noise of these records in comparison to the records of Figs. 4 and 5. Despite the reduced noise, the harmonics up to the fifth order were virtually identical to those obtained at the same frequency with only four pulse pairs averaged. This test also gives further confidence in the frequency and amplitude stability of the voltage-clamp system as outlined above.

In the analyses of the data presented herein harmonics up to the fifth order were found to be above the noise level; the amplitudes of the higher harmonics up to the 30th order were consistently in the range of 0.1 to 0.8% of the amplitude of the fundamental and occurred with random phases from one experimental record to the next. Thus, harmonic amplitudes of $\leq$1% of the fundamental amplitude were considered to be due to noise and were discarded.

Transient Gating Current (Time Domain)

Gating current transients were also obtained by employing the standard P/4 method (Bezanilla and Armstrong, 1977). An example is given in Fig. 3 for a depolarization to 0 mV from the holding potential of −70 mV. Pulse duration was 3 ms with the subtraction holding potential of −170 mV maintained for 20 ms prior to each subtraction pulse. The current records from 10 pulse cycles were averaged. Further examples of transients for two other values of depolarization are given in Fig. 4 of Fohlmeister and Adelman (1985).

RESULTS

Periodic Current Records

Fig. 4 gives gating current records for command sinusoidal voltage changes at 612 Hz about a series of mean membrane potentials. These records were obtained under conditions very near, or at dynamic steady state (see Methods). Note that as the mean membrane potential is increased from −80 mV to values > 0 mV the periodic records become increasingly distorted relative to a pure sine wave at the command frequency. Inspection indicates an increasingly strong second harmonic with depolarization: the second bump within each period appears to be pushing itself upwards with increasing mean membrane potential until it becomes the dominant bump at values of E_{mean} somewhat beyond 0 mV. At the point of dominance exchange the amplitude of the second harmonic is larger than that of the fundamental component (see Figs. 7 and 9 below).

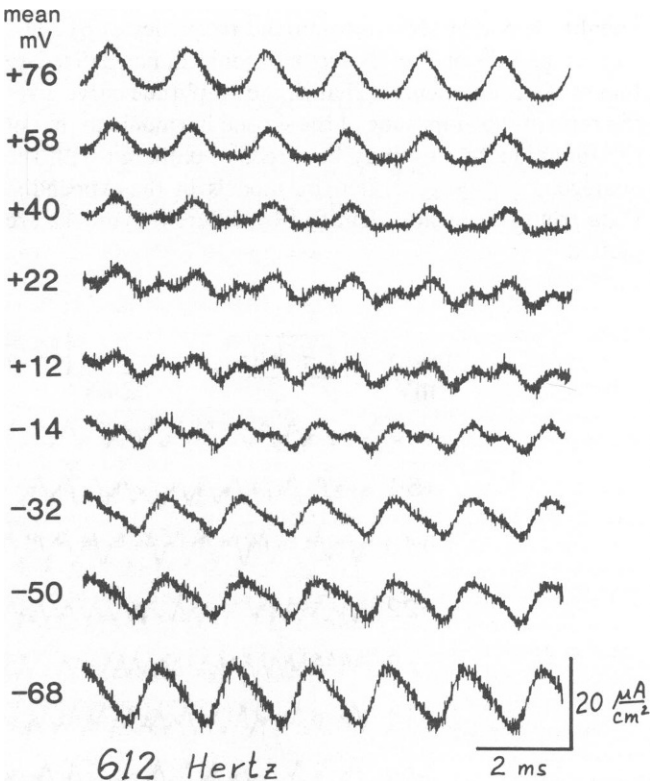

FIGURE 4 Gating current responses to sinusoidal voltage clamp at 612 Hz and ±35 mV amplitude for nine values of E_{mean} given at the *left*. The current traces were obtained during the dynamic-steady-state phase (see text). Four records were averaged to obtain each trace. Note the strong second harmonic for centrally located E_{mean}, and the relatively low distortion near the ends of the experimental range of E_{mean}.

Figs. 5 (left and right) give similar sets of records for command frequencies of 1.4 and 3.0 kHz, respectively. The qualitative features discussed above for Fig. 4 remain unchanged at these higher frequencies.

The Fundamental Component

Fig. 6 gives the absolute amplitude of the fundamental component in the periodic gating current records as a function of E_{mean} and frequency. This amplitude is distinguished by a trough that runs in a direction nearly parallel to the frequency axis for $E_{mean} \sim +10$ mV (see also Fig. 11). The trough deepens and becomes more V shaped with increasing frequency. The location of the trough coincides with the location of dominance exchange between the two peaks in the periodic current records.

The fundamental component amplitude peaks in a rounded ridge that runs parallel to the frequency axis near E_{mean} at about -40 mV. The elevation of this ridge slowly increases with increasing frequency.

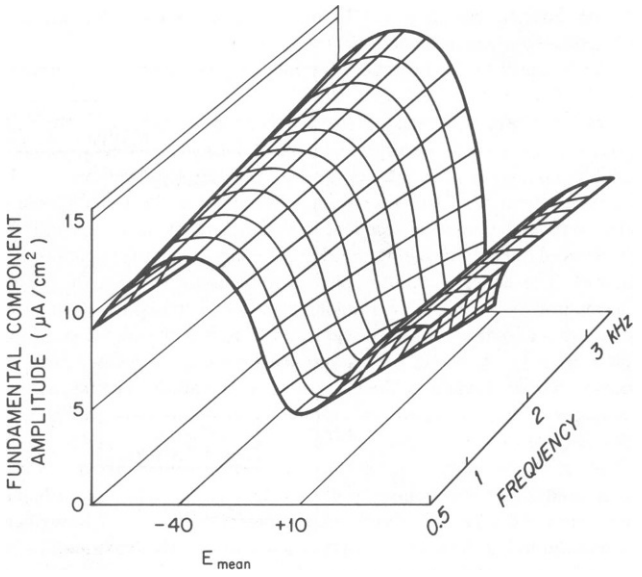

FIGURE 6 Amplitude in $\mu A/cm^2$ of the fundamental component of gating current in dynamic steady state as a function of E_{mean} and command frequency.

Harmonic Analysis

Fig. 7 gives plots of the phases of the fundamental component and the second harmonic as well as of the normalized amplitude of the second harmonic as functions of the mean membrane potential for a command frequency of 612 Hz. The amplitude of the second harmonic is normalized to that of the fundamental. That is, the amplitude curve gives the ratio of the amplitude of the second harmonic to that of the fundamental and may be directly compared with the analogous curves generated by models in the Appendix. Data from two axons, identified by different symbols, are plotted.

The most striking feature in Fig. 7 is the broad and slightly rounded peak in the normalized amplitude of the second harmonic centered on about +10 mV. This feature is in marked contrast to the behavior of the normalized second harmonic in any of the standard models simulated in the Appendix. The normalized amplitude of the second harmonic further showed a tendency to generate a local minimum near about -40 mV. The amount of this dip varied from axon to axon. The two axons whose data are plotted in Fig. 6 show the two extremes of this tendency. For membrane potentials < -60 mV the amplitude

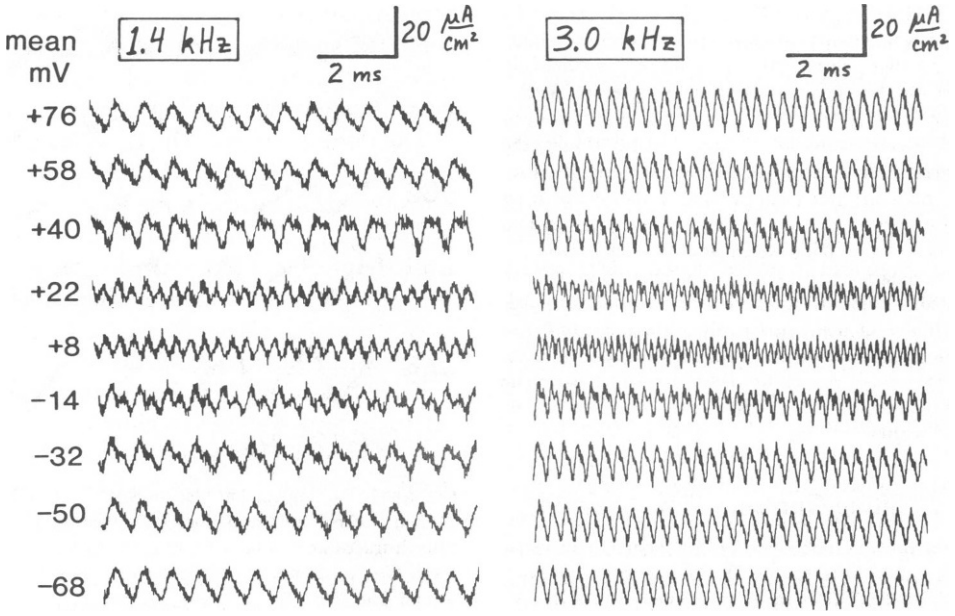

FIGURE 5 Same as Fig. 4, except f = 1.4 kHz (*left*) and f = 3.0 kHz (*right*).

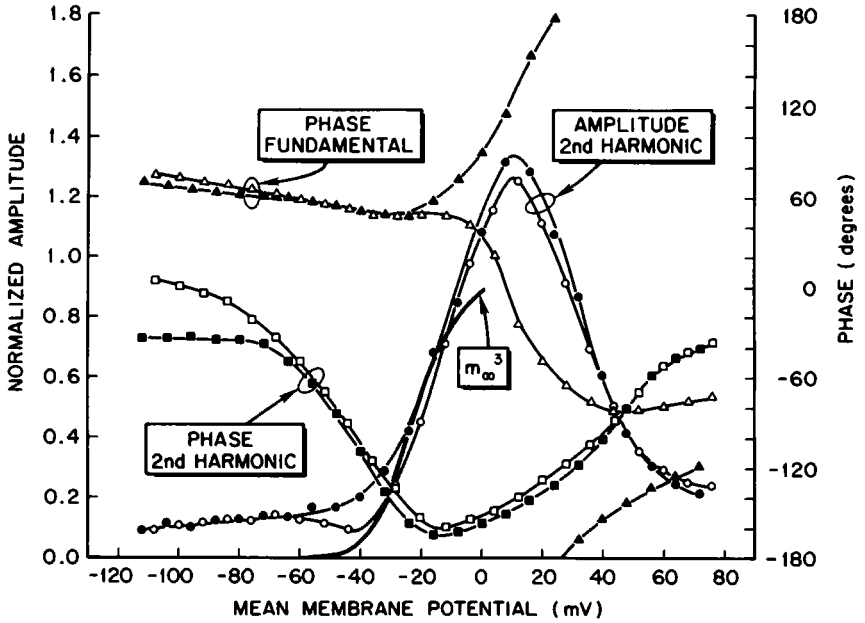

FIGURE 7 Phases of the fundamental component (triangles) and second harmonic (squares), and the normalized amplitude of the second harmonic (circles) of the periodic gating current generated by two axons as functions of E_{mean} in dynamic steady state. The two axons are distinguished by the use of open and filled symbols. Frequency = 612 Hz. The amplitude scale is in dimensionless units giving the ratio of the amplitudes of the second harmonic to that of the fundamental component. Phases are relative to the phase of the command sinusoid. Heavy curvilinear line segment ranging from −60 to 0 mV gives m_∞^3 of the Hodgkin-Huxley model as a function of E. The amplitude scale is also the ordinate scale for this curve.

showed a slow decline towards more negative membrane potentials, at least down to −112 mV. At the upper end of the mean membrane potential range the amplitude appeared to continue to decline at least up to +72 mV.

The phase of the fundamental component initially decreases slowly as E_{mean} is increased, and crosses a value of about +62° at E_{mean} = −80 mV. As E_{mean} approaches 0 mV two types of phase behavior were observed; the slightly more common phase behavior (6 out of 10 axons) for frequencies <1 kHz showed a relatively abrupt decrease to negative phase angles within the domain of 0 to +20 mV. The remaining four axons gave a sharp increase in the fundamental phase to 180°, only to reappear (in wrap-around fashion) at negative phase angles. This sharp phase change also occurred in the domain of 0 to +20 mV. For command frequencies above 1 kHz this second type of phase behavior became more common, occurring in 80% of axons at 5 kHz. In all cases the phase varied most rapidly in the neighborhood of the same value of E_{mean} as the peak in the amplitude of the second harmonic. This qualitative phase behavior of the fundamental component is easily explained; of the two current peaks per sine-wave period, the larger one is more influencial in locating the fundamental component of the Fourier series. Thus, a relatively abrupt change in the phase of the fundamental is expected at the point of dominance exchange between the two current peaks. In any adequate model based on the data herein, the bifurcation in the behavior of the phase of the fundamental should be expressed as a phase instability in the domain of 0 to 20 mV. Such a phase instability implies that certain small parameter changes will be sufficient to convert from one type of behavior to the other.

The phase of the second harmonic declines from slightly negative values at the extreme ends of the experimental range of E_{mean} to a broad minimum with a low point of about −160°. The minimum is asymmetrical with respect to the amplitude peak in the second harmonic, the low point occurring at about −15 mV. The asymmetry and location of the low point were absolutely reproducible from axon to axon. However, there was some variation (±25°) in the phase at the low end of E_{mean} (−112 to −70 mV), indicating, again, a region of instability, in this case an instability in the phase of the second harmonic.

The third harmonic (Fig. 8) shows a well-rounded peak near E_{mean} = −30 mV. The corresponding phase shows a pronounced dip at the same location. For more negative values of E_{mean} the third harmonic is rapidly reduced to the noise level (see Methods). For larger values of E_{mean} (> −10 mV) the normalized amplitude of the third harmonic remains above the noise level, but contains no further distinguishing features.

Fig. 8 also gives a plot of the maximum variation (extreme peak-to-peak amplitude) of the periodic gating current as a function of E_{mean}. Note that this peak-to-peak amplitude remains relatively constant, in sharp contrast to the corresponding amplitude generated by the models in the Appendix.

Fig. 9 gives plots of harmonic variables as in Figs. 7 and 8, but for a command frequency of 3 kHz. The overall picture is similar to that in the earlier figures with the

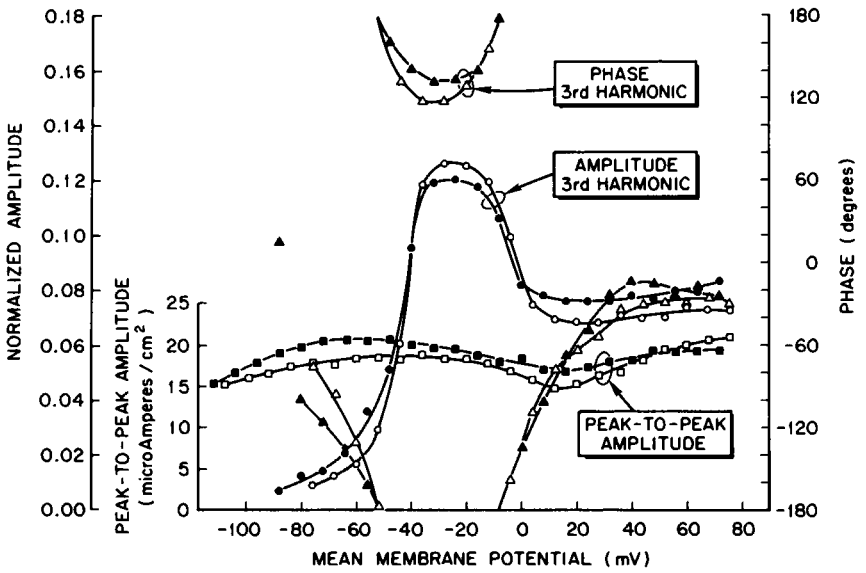

FIGURE 8 Normalized amplitudes and phases (see Fig. 7 caption) of the third harmonic in the periodic gating current for two axons as functions of E_{mean}. Also plotted is the extreme variation (peak-to-peak amplitude) in the gating current within one period of the stimulus in dynamic steady state.

following important changes: (*a*) The peak in the normalized amplitude of the second harmonic rises to larger values and has a more spiked shape. (*b*) The phases of the fundamental and second harmonic are reduced (in degree values), with the exception of the fundamental in the unstable domain of 0 to +20 mV. The phase of the second harmonic is reduced relatively more strongly near the ends of the experimental domain of mean membrane potentials. (*c*) The dominant and rounded peak in the normalized amplitude of the third harmonic near $E_{mean} = -25$ mV has been reduced to the noise level. The peak has been replaced (as dominant feature) by a maximum that is located at the same position in E_{mean} as the peak in the amplitude of the second harmonic.

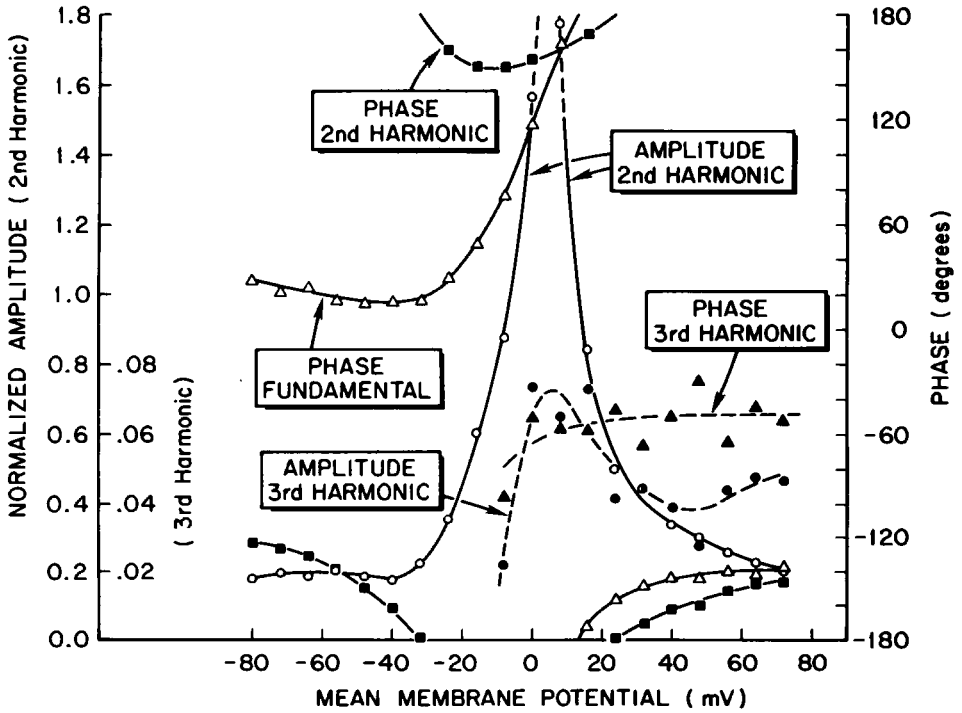

FIGURE 9 Normalized amplitudes and phases (see Fig. 7 caption) up to the third harmonic as functions of E_{mean} for a command frequency of 3 kHz. See text for data interpretation.

Fig. 10 gives (surface) plots of the normalized amplitudes of the second and third harmonics as functions of E_{mean} and frequency. The pointed ridge in the third harmonic, whose crest is positioned near $E_{mean} = +10$ mV, is due entirely to the normalization, and follows the course of the trough in the amplitude of the fundamental component (see Fig. 6). The rounded ridge centered near $E_{mean} = -25$ mV may be correlated with the nonlinear voltage dependence of the rate constants (see Appendix).

Fig. 11 gives plots of the absolute amplitudes of the second and third harmonics as functions of E_{mean} for two widely spaced command frequencies. These plots show that the dominant feature in the second harmonic, which is centered near $E_{mean} = +10$ mV, is a very weak function of command frequency, and that the increasingly spiked shape of the second harmonic ridge with increasing frequency in Fig. 10 is also due to normalization. The third harmonic contains no outstanding features at the highest command frequency (3 kHz). As the frequency is reduced, however, a rounded peak develops near $E_{mean} = -32$ mV; this is the peak that is correlated with the nonlinear voltage-dependence of the kinetic rate constants (c.f. above and Appendix).

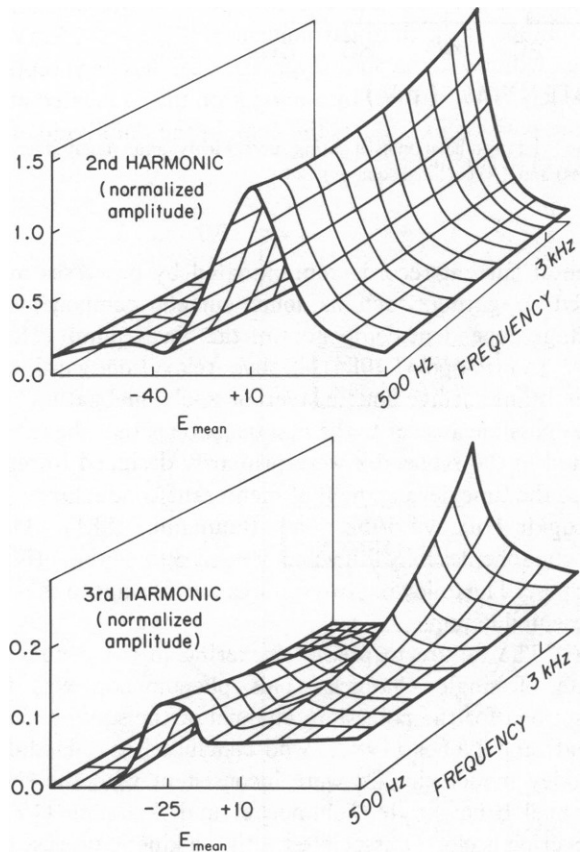

FIGURE 10 Normalized amplitudes of the second harmonic (*upper* plot) and the third harmonic (*lower* plot) of gating current in dynamic steady state as functions of E_{mean} and command frequency. Values are plotted as dimensionless ratios of (harmonic amplitude/fundamental-component amplitude).

DISCUSSION

The dominant feature in the data is a pronounced peak in the amplitude of the second harmonic as a function of E_{mean}. Equally notable by their absence are substantial second harmonic components for $E_{mean} < -40$ mV and $E_{mean} > 30$ mV generated by standard gating kinetic models whose simulations are given in the Appendix. The source of these strong, model generated harmonics can be inferred by inspection of the model-generated records; the strong second harmonics reflect the models' inability to continue to generate gating currents beyond a relatively narrow range of membrane potentials due to their kinetic structure and rate constants. When the voltage swings outside of that range, the models simply run out of molecular states and no further kinetic transitions are possible. As a result the periodic gating current is highly distorted. The reduced ability to generate gating currents is reflected in the small peak-to-peak amplitude of the simulated model current records (for details see Appendix).

The experimental data show no such distortions, presumably because the actual Na-channel activation kinetics are not so restricted by kinetic end states, and are therefore able to continue to generate gating current outside of what may be considered the model gating range of roughly -60 to $+20$ mV (c.f. the curve segment that gives $m_\infty^3(E)$ in Fig. 7). Further, the peak-to-peak amplitude of the experimental gating currents remains relatively constant at all voltages (Fig. 8). To reconcile this particular difference between the models and the data is a relatively simple task (c.f. Fohlmeister and Adelman, 1985) once the source of the model behaviors is understood.

However, the models simulated in the Appendix are of little help in attempts to interpret the peak in the second harmonic seen in the data. This peak is in reality a ridge if command-frequency is considered as a second independent variable (see Fig. 10). The ridge is due to the second upswing, or bimodal shape within the periodic current records, that occurs for all frequencies within a relatively wide band whose width extends from either side of $E_{mean} = +10$ mV. The bimodal shape strongly suggests that this second harmonic component is not due to kinetic end-state saturation because saturation leads to plateaus in the current records. The interpretation of the biomodal shape must be consistent with the following two observations: (*a*) The weak frequency dependence of the bimodal shape implies that the temporal spacing between the two peaks is approximately inversely proportional to the command frequency, and is therefore not constant. (*b*) The approximate locations of the two peaks with respect to the phase of the command sinusoid can be estimated from the phase of the fundamental component in regions of E_{mean} where one or

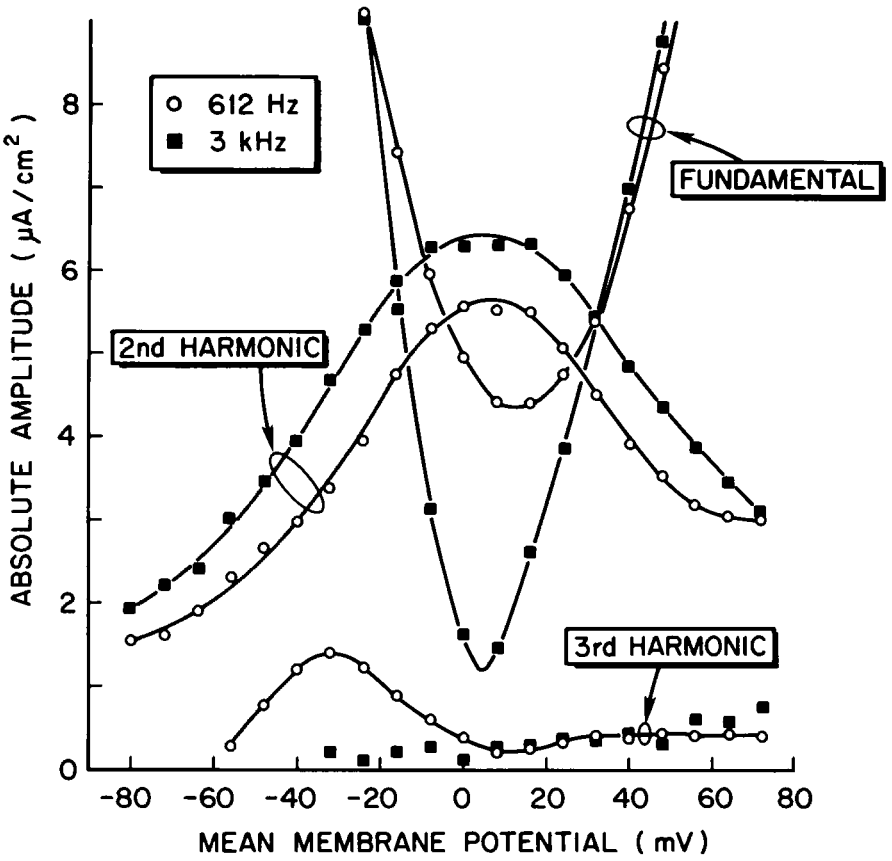

FIGURE 11 Amplitudes in $\mu A/cm^2$ of the fundamental component, the second and third harmonics of gating current in dynamic steady state as functions of E_{mean} for the two command frequencies of 612 Hz (open circles) and 3 kHz (filled squares).

the other of the peaks dominate (see Figs. 7 and 9). Whereas the first peak occurs during the rising (depolarizing) phase, the second peak occurs during the falling phase of the sinusoid. Since a current peak implies a positive (outwardly directed) current, the two peaks contribute components of the opposite sign to the gating current.

These observations strongly suggest the operation of two coupled molecular processes, with independent degrees of freedom in their movement, on electrostatic grounds (see Fohlmeister and Adelman, 1985). Kinetics based on this interpretation, as well as a model gate based on the recently determined primary structure of the Na channel (Noda et al., 1984), are developed in Fohlmeister and Adelman (1985).

The remaining question deals with the evidence contained in the harmonic data that gating currents are due to the rate of change of membrane surface polarization in response to kinetic transitions associated with the sodium-activation gating mechanism. This evidence alone is by no means conclusive; rather, it demonstrates the consistency of that interpretation. The question is divided into the following two components: (*a*) Why do kinetic models designed to describe membrane excitability fail when tested for their gating current response under conditions of dynamic steady state? (*b*) To what extent are the experimental current records contaminated by processes unrelated to gating, such as ionic current components, a voltage-dependent component of the Na-K pump (Holloway and Poppele, 1984), Debye relaxation within the membrane surface double layer, or K-channel gating?

A possible answer to the first question is that the models tested in the Appendix were primarily designed to reproduce the time development of membrane conductance (c.f. Hodgkin-Huxley, 1952; and Baumann, 1981). Those kinetic schemes may fail when pressed beyond that original purpose. The following two failures are relevant to the data presented herein:

(i) The failure to predict flickering in the conducting state of single channels. This phenomenon was first described for the potassium channel of the squid axon by Conti and Neher (1980), who concluded that Hodgkin-Huxley model kinetics were inconsistent with the single channel behavior. In Fohlmeister and Adelman (1985), flickering is closely associated with the kinetic process that generates the peak in the second harmonic, a feature that is absent in simulations of the Hodgkin-Huxley model (c.f. Appendix).

(ii) The second failure lies in two observations that might appear to be unrelated. It was first observed that sizeable gating currents are generated in the hyperpolar-

ized region of membrane potentials. Subsequently a small Cole-Moore (1960) type shift was found in sodium activation following voltage steps from hyperpolarized prepotentials (Taylor and Bezanilla, 1983). This Cole-Moore type shift is accompanied by a sizeable increase in the gating current (Taylor and Bezanilla, 1983). We employ a version of the Hodgkin-Huxley model to illustrate the source of the model's failure to predict these phenomena. The version used is given by the kinetics:

$$x_1 \underset{\beta_m}{\overset{3\alpha_m}{\rightleftharpoons}} x_2 \underset{2\beta_m}{\overset{2\alpha_m}{\rightleftharpoons}} x_3 \underset{3\beta_m}{\overset{\alpha_m}{\rightleftharpoons}} x_4.$$

The steady state population probabilities of the states x_i at -60 mV are $x_1 = 0.849$, $x_2 = 0.142$, $x_3 = 0.00796$, $x_4 = 0.000148$ where $\Sigma x_i = 1$. Note that the state x_1 is the dominantly populated one at -60 mV. Therefore, there is only a small possibility of further kinetic transitions to the left following hyperpolarization. As a result there is a very little gating current in response to a hyperpolarizing voltage step, there will be virtually no Cole-Moore shift, and no significant increase in the predicted gating current with prehyperpolarization. This difficulty was removed by increasing the number of sequential kinetic states beyond those given by the Hodgkin-Huxley model (c.f. Armstrong and Bezanilla, 1977). In Fohlmeister and Adelman (1985) we show that the harmonic data suggest a similar increase in the number of required sequential substates, thus establishing a further link between gating current data obtained in the time domain and the present harmonic analysis.

The dynamic data do, however, suggest one further feature that has not yet been reported in the transient, time-domain data: In Fohlmeister and Adelman (1985) we show that kinetics based on the harmonic data can result in an undershoot (inwardly directed current) following the early and large outwardly directed gating current transient in response to large depolarizations.

To the question of contamination of the current records by processes unrelated to gating kinetic transitions we can give no precise answer at this time. Because of the complex structure of the axonal membrane it is very likely that at least some contamination is present due to other voltage-sensitive processes. Nevertheless, the harmonic data contain a number of indications that the basic features of those data are due to activation-gating kinetics: (*a*) The values of the phase angle of the fundamental component for $E_{mean} < -20$ mV are characteristic of kinetics with rate constants whose values give the known gating times for sodium activation. This is indicated by all of the model simulations carried out in the Appendix as well as for the model given in Fohlmeister and Adelman (1985). In other simulations carried out with the latter model we found that when all of the primary rate constants were increased (or decreased) by a factor of two the phase angle of the fundamental component increased (or decreased) by ~14° respectively. The reduction in the fundamental phase for higher command frequencies seen in Fig. 9 is due to the same phenomenon because frequency and rate constant commonly appear as a ratio in analytical expressions for phase in any frequency-domain analysis (c.f. Fernandez, Bezanilla, and Taylor, 1982). (*b*) In comparing the second harmonic behavior of the Hodgkin-Huxley model with the data near $E_{mean} = -35$ mV, there is some indication that the slight dip in the normalized amplitude seen experimentally is due to the same type of kinetic process that produces the sharp minimum in amplitude and rapid phase change in the Hodgkin-Huxley model simulations. The model simulations in Fohlmeister and Adelman (1985) were carried out for the specific purpose of fitting the data. However, the reproduction of the small dip in amplitude was not considered to be of fundamental importance for that purpose. Nevertheless, the basic model has a tendency to generate that local minimum whenever model parameters are chosen to approximate the axonal data. Therefore it is likely that the axon's tendency to show the same local minimum is due to gating kinetics rather than another, unspecified membrane process. (*c*) The amplitude of the third harmonic shows a rounded peak centered at $E_{mean} \approx -42$ mV for the Hodgkin-Huxley model and a corresponding rounded peak near $E_{mean} \approx -30$ mV in the experimental data. These peaks are the most striking features of the third harmonic in both the data and the Hodgkin-Huxley model. The presence of that peak in the model data is known to be due to the particular nonlinear voltage dependence of the model rate constants, and vanishes if that voltage dependence is linearized during the sinusoidal oscillation (see Appendix). The similarity in the peaks again suggests a gating-kinetic origin for the experimental gating currents.

It is somewhat unfortunate that all three of the above points describe similarities between kinetic models and experimental data in the same region of E_{mean}. The disagreement for more negative values of E_{mean} has already been explained without the need of any fundamental change in the primary gating kinetics. For more depolarized values of E_{mean} near the peak of the normalized second harmonic we find another type of correlation between the Hodgkin-Huxley model and the data: the rate of increase of the amplitude of the second harmonic as a function of E_{mean} is very nearly proportional to the rate of increase of m_∞^3 as a function of E (Fig. 7). This suggests that the secondary kinetics responsible for that harmonic may be associated with the actual opening of the activation gates, and that the molecular changes associated with the primary kinetics determine the probability of that opening transition. This concept is further developed in Fohlmeister and Adelman (1985).

APPENDIX

Model Gating Current in Dynamic Steady States

A number of model activation gating kinetics were subjected to simulated sinusoidal voltage changes of 35 mV (70 mV peak to peak) amplitude

about a set of values of E_{mean} (-80 mV $\leq E_{mean} \leq +$ 72 mV) and for various frequencies f, $0.5 \leq f \leq 5$ kHz. The model molecular conformational states, herein denoted by x_i, were the dependent variables (functions of time, t) of the coupled, first order kinetic differential equations that were integrated using a Runge-Kutta routine on a Cyber 845 computer (Control Data Corp., Minneapolis MN). The initial conditions of the functions $x_i(t)$ were set somewhat arbitrarily, subject to overall population constraints (e.g. Eqs. 2) that were maintained throughout the integrations. For each value of E_{mean} the functions, $x_i(t)$, approached a periodic waveform (with the period of the command sinusoid) on a timescale of ~2 ms; this asymptotically approached periodic waveform was independent of the initial conditions. The numerical integration was continued until every variable x_i returned to the same value at the end of a sine wave period that it had at the beginning of the period to within 0.1% of the total variation of that variable during the period. This condition was defined as (near) "dynamic steady state."

Single periods of the simulated gating current records in dynamic steady state were sampled at 16 equally spaced points covering the period. On the basis of the 16 points, an FFT routine computed the real and imaginary parts of the DC component, the fundamental component and of each of the harmonics of orders two through six. These parts were converted to amplitudes and phases (relative to the phase of the command sinusoid). Trial Fourier analyses based on 64 points per period yielded harmonic components up to 30th order. In these trials the harmonic content up to the sixth order was virtually identical to that obtained with 16 points per period. Furthermore, harmonic amplitudes of order ≥ 6 were consistently in the range of <0.01 of the fundamental component, and in most cases were virtually zero. Thus, for the types of functions that represent gating currents in sinusoidally driven dynamic steady states, the Fourier series converges rapidly, although the amplitude of the second and third harmonic can be sizeable and indeed larger than that of the fundamental.

As a final test, electronically generated (shot) noise was subjected to Fourier analysis; the resulting spectrum was relatively flat up to the 30th harmonic component, which was the highest component determined in the analysis. When this noise was added to a simulated gating current record (RMS amplitude 20% of the amplitude of the current record) the low order (≤ 5) harmonics in the noisy current record were virtually identical to those in the control current record.

The Hodgkin-Huxley Model

Two kinetic versions of the sodium-activation component of the Hodgkin-Huxley (1952) model were simulated. The kinetics are given by

$$x_1 \underset{\beta_m}{\overset{3\alpha_m}{\rightleftharpoons}} x_2 \underset{2\beta_m}{\overset{2\alpha_m}{\rightleftharpoons}} x_3 \underset{3\beta_m}{\overset{\alpha_m}{\rightleftharpoons}} x_4 \tag{1a}$$

and by

$$x_1 \underset{\beta_m}{\overset{\alpha_m}{\rightleftharpoons}} x_2. \tag{1b}$$

Population constraints for schemes 1a and 1b were

$$x_1 + x_2 + x_3 + x_4 = 1.0 \tag{2a}$$

and

$$x_1 + x_2 = 1.0, \tag{2b}$$

respectively. The simulated gating current is proportional to

$$i_g = 3\alpha_m x_1 + 2\alpha_m x_2 + \alpha_m x_3 - 3\beta_m x_4 - 2\beta_m x_3 - \beta_m x_2 \tag{3a}$$

for scheme 1a and to

$$i_g = \alpha_m x_1 - \beta_m x_2 \tag{3b}$$

for scheme 1b.

Although the kinetics of scheme 1a and scheme 1b and their associated gating current simulations (Eqs. 3) appear to be quite different in structure, the waveform of the periodic gating current, $i_g(t)$ generated by them in dynamic steady state, and their harmonic content is absolutely identical. This is so despite the fact that the open state, x_2, for scheme 1b must be cubed in order to give the relative sodium conductance, whereas the open state, x_4, for scheme 1a is proportional to sodium conductance directly.

Fig. 12 *A* gives the simulated gating current responses of the Hodgkin-Huxley model for a series of E_{mean} for one period of the stimulus sinusoid in dynamic steady state. Note that the current records are least distorted (relative to a pure sine wave) for values of E_{mean} near -35 mV. For other values of E_{mean} the current records in Fig. 12 *A* show plateaus.

Figs. 12 *B* and *C* give plots of the harmonic amplitudes and phases up to the third harmonic of the current records in Fig. 12 *A* as functions of E_{mean}. Note that in a very narrow range of E_{mean} where the current records are least distorted, the largest distortion is in the third harmonic. Elsewhere, the dominant distortion lies in the second harmonic, although the third harmonic can also be large.

Also plotted in Fig. 12 *C* is the extreme peak-to-peak amplitude of the gating current within one period. Note that this amplitude is roughly bell shaped and peaks for the value of E_{mean} at which the second harmonic reaches its minimum.

Fig. 13 gives the low-order harmonic content in the periodic gating current for a command frequency of 2.5 kHz. The general pattern is similar to that found for f = 500 Hz. The principal differences are that the features in the curves as functions of E_{mean} are somewhat softened, and the phases are somewhat reduced at the higher command frequency. The softening of the features is due to a general reduction in the amplitudes of the harmonic components relative to the fundamental. This is equivalent to a more linear response at the higher command frequency. This frequency-dependent behavior was observed for all model kinetics that were simulated.

Other Kinetic Models

Kinetic equations of gating models that contain mathematical features not found in the Hodgkin-Huxley equations were also integrated in dynamic steady states and the simulated gating currents subjected to harmonic analyses. These models included aggregation gating (Baumann, 1981) and an excited state model (Jakobsson, 1978). The aggregation kinetic equations contain nonlinear terms (i.e., products of dependent variables of the form $x_i x_j$) and the excited state model contains one rate constant whose value depends on the rate of change of the membrane potential. Despite these unique features the qualitative behavior of the gating current generated by them in dynamic steady states is similar in its harmonic content to that of the Hodgkin-Huxley model (see Summary of Model Generated Harmonic Behavior below). This qualitative similarity is the basis for considering these models to be dynamically equivalent, and this equivalence class is represented by a very simple kinetic model that is its prototype. This prototype model contains only those ingredients that are necessary to generate the basic harmonic features common to its class: The model has two kinetic states (conformations) and two voltage-dependent rate constants

$$x_1 \underset{k_{21}}{\overset{k_{12}}{\rightleftharpoons}} x_2.$$

The rate constants were given the form

$$k_{12}(E) = (1.6) \exp [0.028\ (E + 36)] \tag{4a}$$

$$k_{21}(E) = (1.6) \exp [-0.028\ (E + 36)] \tag{4b}$$

in order to generate the simulated harmonics in Fig. 14. The overall factor of 1.6 ms^{-1} was chosen almost at random to give the rate constants a value that roughly corresponds to the rate of Na channel activation gating at 8°C. This value can be changed significantly without affecting the basic harmonic features. This relative insensitivity is the reason for the very

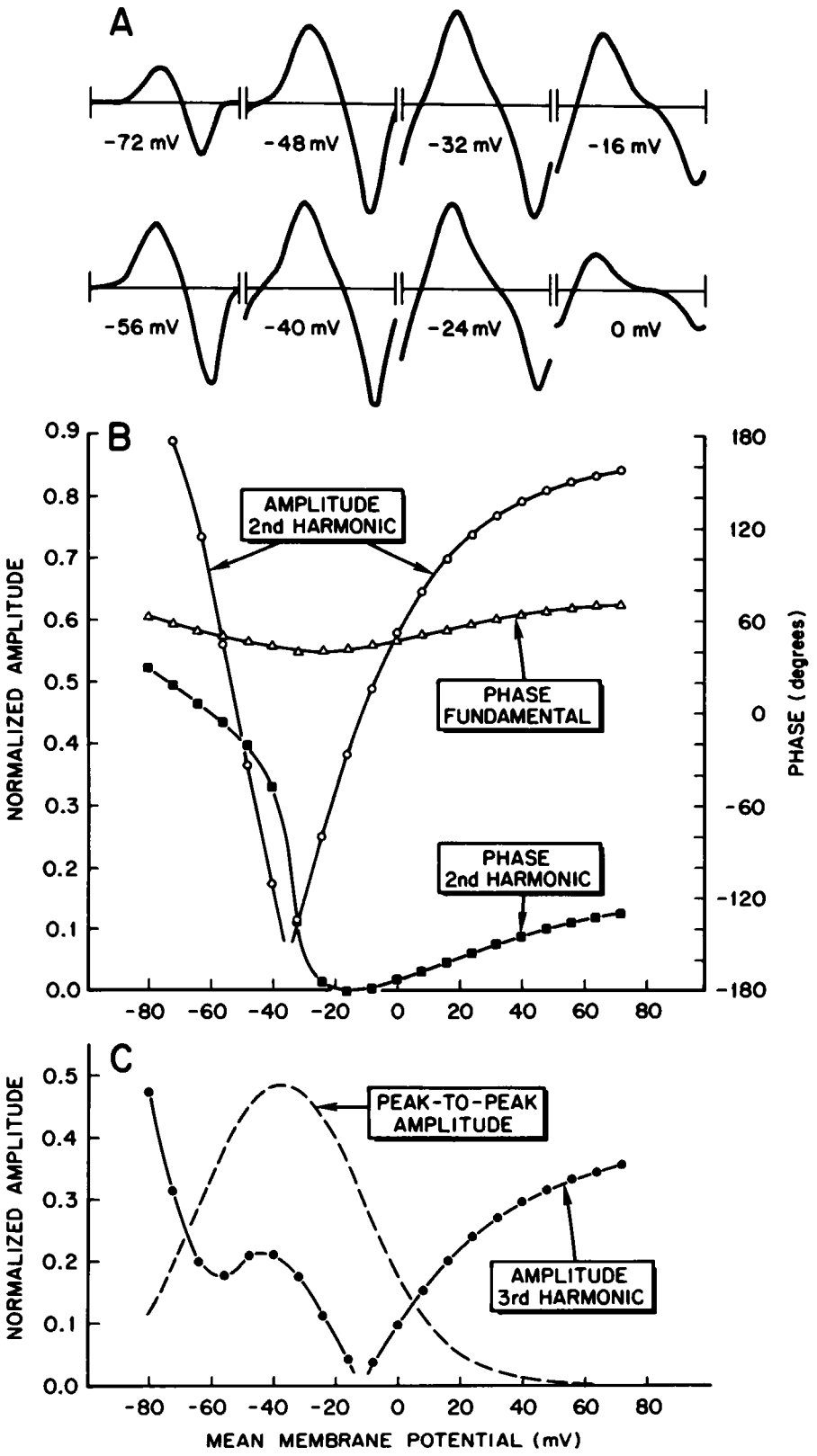

FIGURE 12 (*A*) Simulated gating current records generated by the Na-activation component of the Hodgkin-Huxley model kinetics in dynamic steady states about a series of E_{mean} that identifies each trace. f = 500 Hz.
(*B*) Phases of the fundamental component and second harmonic and normalized amplitude of the second harmonic of gating current generated by Hodgkin-Huxley model kinetics in dynamic steady states as functions of E_{mean} for f = 500 Hz.
(*C*) Normalized amplitude of the third harmonic for conditions as in *B*. Also plotted is the peak-to-peak amplitude of the periodic currents (dashed curve).

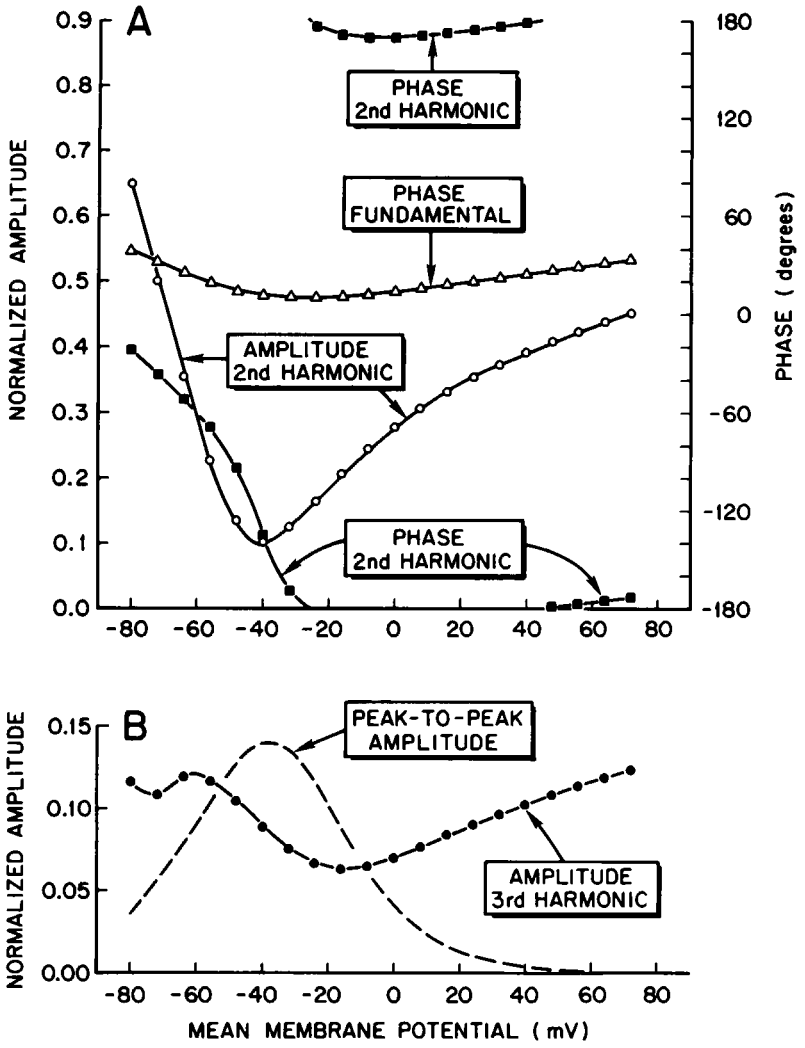

FIGURE 13 (*A*) and (*B*) Same as Fig. 12 *B* and *C*, respectively, except f = 2.5 kHz.

weak functional dependence of the harmonic content on command frequency (c.f. Figs. 12 and 13), a property common to all models that were simulated, and, indeed, also found in the experimental data.

All of the plotted harmonic elements (amplitudes and phases)—except the phase of the second (and higher even ordered) harmonic—are mirror images about $E_{mean} = -36$ mV. This is due to the fact that the rate constants k_{12} and k_{21} go over one into the other with the replacement $(E + 36) \rightleftharpoons -(E + 36)$. The symmetry point $E_{mean} = -36$ mV was chosen because that is near the center of the gating range of the Hodgkin-Huxley model; at that point the forward, k_{12}, and backward, k_{21}, rate constants of the prototype model are equal. Voltage oscillations of moderate amplitude (± 35 mV) about -36 mV produce the least amount of distortion in the gating current because there is little constraint on the possibility of shifting the population between conformational states x_1 and x_2 throughout the sinusoidal cycle. As E_{mean} moves away from -36 mV, either state x_1 or x_2 becomes increasingly more dominantly populated. During certain phases of the sinusoidal voltage oscillation about such side values of E_{mean} the population of either state x_1 or x_2 approaches saturation and no further kinetic transitions or gating current is possible until after the phase of the command sine wave reverses direction. This phenomenon leads to plateaus in the periodic gating currents as seen in Fig. 12. The harmonic content of such plateau current records is expressed in a large second harmonic and a somewhat smaller third harmonic. Furthermore, the peak-to-peak amplitude of the gating current is markedly reduced due to the severe restriction on the possibility of kinetic transitions for E_{mean} near the ends of the simulation domain.

The phase of the second harmonic makes an abrupt jump of 180° at $E_{mean} = -36$ mV in Fig. 14. This is due to the sudden change in the location of the plateaus in the gating current records between outwardly and inwardly directed phases of the current. This phenomenon is observed in the current records of Fig. 12 for the Hodgkin-Huxley model kinetics, although the phase transition in the second harmonic is not quite so abrupt there as in the prototype model.

The minimum in the amplitude of the second harmonic is narrower for the Hodgin-Huxley model kinetics (Fig. 12) than it is for the prototype model (Fig. 14). In other words, the amplitude of the second harmonic is a stronger function of E_{mean} in the former model than in the latter. This is due to the weaker voltage dependence of the rate constants of the prototype model as compared to that of the Hodgkin-Huxley model. The voltage dependence of the rate constants k_{12} and k_{21} can be increased by increasing the magnitude of the coefficients (the factors 0.028 and -0.028) of $E + 36$ in the exponents of Eqs. 4. In general, the valley in the amplitude of the second harmonic can be widened by either reducing the voltage dependence of the rate constants, or by adding further sequential kinetic states to the kinetic scheme with appropriately chosen values for the rate constants (see Fohlmeister and Adelman, 1985).

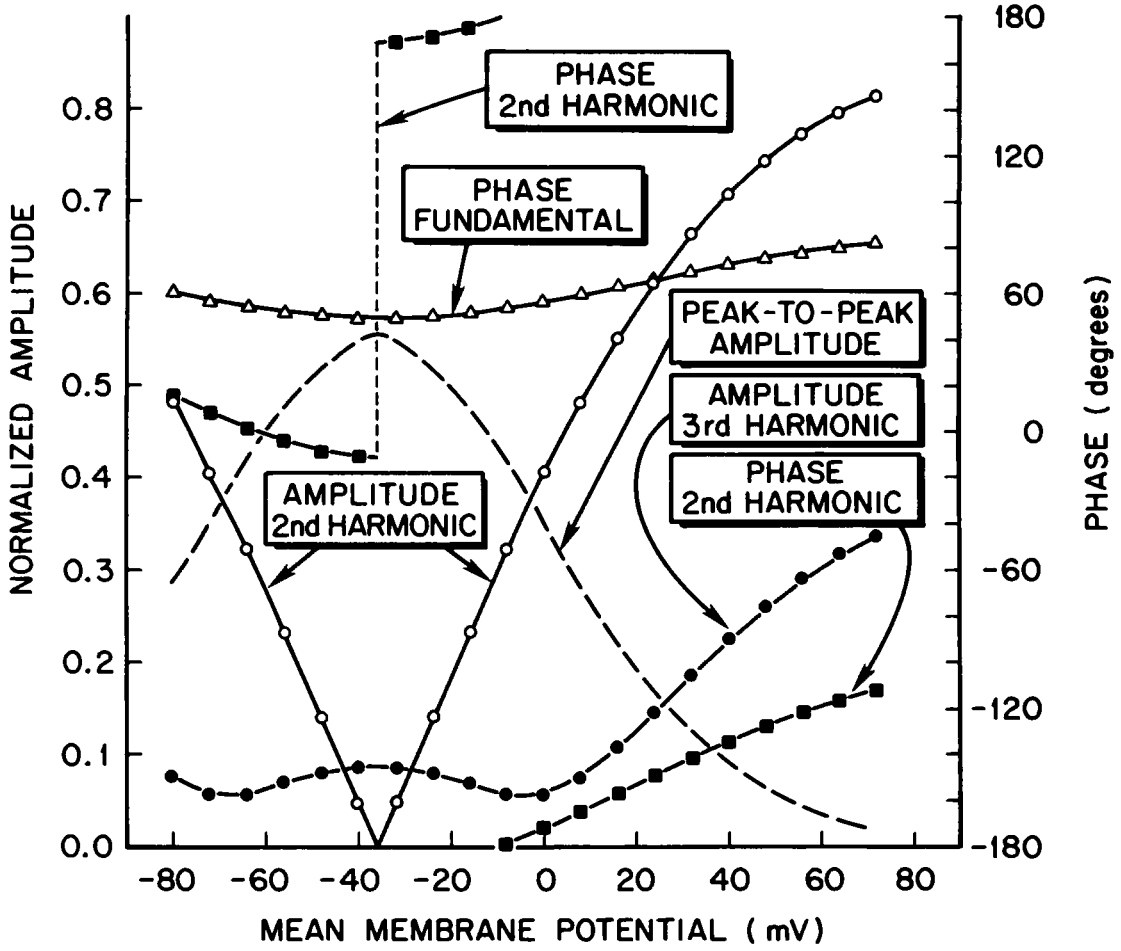

FIGURE 14 Phases and normalized amplitudes of harmonic components generated by the prototype model (Eqs. 4) of the dynamic-equivalence class that contains the Hodgkin-Huxley model as a member. See text for details.

Finally, the local maximum in the amplitude of the third harmonic near the location of the minimum of the second harmonic was found to be due to the exponential (i.e., nonlinear) voltage dependence of the rate constants as they are varied throughout the sinusoidal cycle. Because of the nonlinear E dependence there occurs a surge of gating current at the extremes of the command sinusoidal swings for values of E_{mean} that are not encumbered by end-state saturation (see Fig. 12 *A*). This surge current gives a distortion that is expressed as third harmonic. When the (local) variation of the rate constants about each value of E_{mean} is linearized to the forms

$$k_{12}(t) = k_{12}(E_{mean})\,[1 + 0.67 \sin 2\pi ft] \qquad (5a)$$

$$k_{21}(t) = k_{21}(E_{mean})\,[1 - 0.67 \sin 2\pi ft] \qquad (5b)$$

then the local maximum in the third harmonic amplitude vanishes, and that amplitude approaches zero at $E_{mean} = -36$ mV for the prototype model. Other salient harmonic features remain unaltered.

Summary of Salient Model Harmonic Features

(*a*) The peak-to-peak variation of the simulated gating current as a function of E_{mean} is roughly bell shaped. That peak-to-peak current amplitude shows a strong and broad peak centered at E_{mean} approximately equal to -35 mV.

(*b*) The phase of the fundamental component is a relatively constant function of E_{mean}. The value is reduced in a broad and shallow minimum near the center of the simulation range of E_{mean}. The minimum phase value is some 20 to 25° smaller than the end values.

(*c*) The amplitude of the second harmonic shows a dramatic minimum for E_{mean} of about -35 mV. The amplitude increases from that minimum to values that are comparable to the amplitude of the fundamental component. All harmonic amplitudes given herein are normalized to the amplitude of the fundamental component and are therefore given as dimensionless fractions (occasionally larger than 1.0 in value).

(*d*) The phase of the second harmonic declines from a positive value less than the phase of the fundamental as E_{mean} is increased from ≤ -80 mV. The phase then undergoes a relatively abrupt transition at the location of the minimum of the second harmonic amplitude. The transition can take the form of either a steep reduction in the phase angle or a sharp rise in the value of that angle. For either case the phase ultimately shows a moderate rate of increase within the range of large negative phase angles as E_{mean} is further increased.

(*e*) The amplitude of the third harmonic shows a local maximum near the location of the minimum in the amplitude of the second harmonic. This local maximum is due to the nonlinear voltage dependence of the rate constants.

(*f*) The effect of increasing the command frequency is to make the gating current response more linear; the normalized amplitudes of the harmonics decline with increasing frequency. Simultaneously, the phases of the fundamental and harmonic components are reduced in degree

values. Apart from this there are no other outstanding frequency-dependent effects.

Experiments were performed at the Marine Biological Laboratory in Woods Hole, Massachusetts. The authors acknowledge the expert assistance of Mr. Richard M. Waltz in the computer acquisition and processing of the data.

Jurgen F. Fohlmeister was supported in part through research grant BNS-8415181 from the National Science Foundation.

Received for publication 18 March 1985 and in final form 23 May 1985.

REFERENCES

Armstrong, C. M., F. Bezanilla, and E. Rojas. 1973. Destruction of sodium conductance inactivation in squid axons perfused with pronase. *J. Gen. Physiol.* 62:375–391.

Armstrong, C. M., and F. Bezanilla. 1977. Inactivation of the sodium channel II: Gating current experiments. *J. Gen. Physiol.* 70:567–590.

Baumann, G. 1981. Novel kinetics in the sodium conductance system predicted by the aggregation model of channel gating. *Biophys. J.* 35:699–705.

Bezanilla, F., and C. M. Armstrong. 1977. Inactivation of the sodium channel I. Sodium current experiments. *J. Gen. Physiol.* 70:549–566.

Cole, K. S., and J. W. Moore. 1960. Potassium ion current in the squid giant axon: dynamic characteristic. *Biophys. J.* 1:1–14.

Conti, F., and E. Neher. 1980. Single channel recordings of K^+ currents in squid axons. *Nature (Lond.)* 285:140–143.

Fernandez, J. M., F. Bezanilla, and R. E. Taylor. 1982. Distribution and kinetics of membrane dielectric polarization II. Frequency domain studies of gating currents. *J. Gen. Physiol.* 79:41–67.

Fohlmeister, J. F., and W. J. Adelman. 1984. Rapid sodium channel conductance changes during voltage-clamp steps in squid giant axons. *Biophys. J.* 45:513–521.

Fohlmeister, J. F., and W. J. Adelman. 1985. Gating current harmonics II: model simulations of axonal gating currents. *Biophys. J.* 48:391–400.

Hodgkin, A. L., and A. F. Huxley. 1952. A quantitative description of membrane current and its application to conduction and excitation in nerve. *J. Physiol. (Lond.)* 117:500–544.

Holloway, S. F., and R. E. Poppele. 1984. Post-tetanic hyperpolarization evoked by depolarizing pulses in crayfish stretch receptor neurones in tetrodotoxin. *J. Physiol. (Lond.).* 356:343–360.

Jakobsson, E. 1978. A fully coupled transient excited state model for the sodium channel I. Conductance in the voltage clamped case. *J. Math. Biol.* 5:121–142.

Keynes, R. D., and E. Rojas. 1976. The temporal and steady-state relationship between activation of the sodium conductance and movement of the gating particles in the squid giant axon. *J. Physiol. (Lond.).* 255:157–189.

Noda, M., S. Shimizu, T. Tanabe, T. Takai, T. Kayano, T. Ikeda, H. Takahashi, H. Nakayama, Y. Kanaoka, N. Minamino, K. Kangawa, H. Matsuo, M. A. Raftery, T. Hirose, S. Inayama, H. Hayashida, T. Miyata, and S. Numa. 1984. Primary structure of *Electrophorus electricus* sodium channel deduced from cDNA sequence. *Nature (Lond.).* 312:121–127.

Taylor, R. E., and F. Bezanilla. 1983. Sodium and gating current time shifts resulting from changes in initial conditions. *J. Gen. Physiol.* 81:773–784.